Quantum Magnetic Properties and Metal-to-Insulator Transition in Chemically Doped Calcium Ruthenate Perovskite

Deepak K. Singh,* Arthur Ernst, Vitalii Dugaev, Yiyao Chen, and Jagath Gunasekera

Ruthenates provide a comprehensive platform to study a plethora of novel properties, such as quantum magnetism, superconductivity, and magnetic fluctuation mediated metal–insulator transition (MIT). Herein, an overview of quantum mechanical phenomenology in calcium ruthenium oxide with varying compositions is provided. While the stoichiometric composition of $CaRuO_3$ exhibits non-fermi liquid (FL) behavior with quasi-criticality, chemically doped compounds depict prominent signatures of quantum magnetic fluctuations at low temperature that in some cases are argued to mediate in metal–insulator transition. In the case of cobalt-doped $CaRuO_3$, an unusual continuum fluctuation is found to persist deep inside the glassy phase of the material. These observations reflect the richness of the ruthenate research platform in the study of quantum magnetic phenomena of fundamental importance.

1. Introduction

Perovskite magnetic materials are at the frontline of solid-state physics research. Experimental and theoretical exploration of perovskite magnets has resulted in numerous novel discoveries of both fundamental and practical importance.[1] Some of the notable examples include the depiction of high-temperature superconductivity,[2] colossal magnetoresistance,[3] high-efficiency electrodes,[4] and quantum magnetic phenomena.[5–7] Among various perovskite magnets, ruthenates are of special importance as a host of physical and magnetic properties are discovered in materials with varying stoichiometry.[8] Calcium ruthenium oxide with

1-1-3 phase composition is one of the most studied yet not well-understood compounds.[9–17] It is a non-FL metal on the verge of magnetic instability.[14,18–20] Chemical substitution on Ca or Ru site is known to cause metal–insulator transition (MIT) with complex magnetic properties, including spin glass and spin liquid phenomena.[11,21–25] Here, we briefly discuss electrical, magnetic, and spin–spin correlation properties in stoichiometric $CaRuO_3$ and some of the chemically doped versions.

1.1. Electrical and Magnetic Properties of $CaRuO_3$

The perovskite compound crystallizes in the orthorhombic structure (Pnma crystallographic group) with lattice parameters of $a = 5.545$ Å, $b = 7.673$ Å, and $c = 5.398$ Å.[9,12,14,22,26] The octahedral crystalline electric field splits the fivefold degeneracy of Ru $4d^4$ into (t_{2g}^4 and empty e_g, thus resulting in a low-spin electronic configuration.[11,13] There are two peculiar characteristics attested to $CaRuO_3$: magnetic instability (close to magnetic stability) and non-FL behavior. Unlike the ferromagnetic Sr counterpart $SrRuO_3$,[9] $CaRuO_3$ is nonmagnetic.[22] Detailed investigation of underlying magnetism using nuclear magnetic resonance (NMR) measurements revealed a highly dynamic ground state with fluctuating Ru spins at low temperature.[27] Similarly, previous electrical measurements on polycrystalline

D. K. Singh, Y. Chen, J. Gunasekera
Department of Physics and Astronomy
University of Missouri
Columbia, MO 65211, USA
E-mail: singhdk@missouri.edu

A. Ernst
Max-Planck-Institut für Mikrostrukturphysik
Weinberg 2, 06120 Halle, Germany

The ORCID identification number(s) for the author(s) of this article can be found under https://doi.org/10.1002/pssb.202100503.

A. Ernst
Institut für Theoretische Physik
Johannes Kepler Universität
4040 Linz, Austria

V. Dugaev
Department of Physics and Medical Engineering
Rzeszów University of Technology
35-959 Rzeszów, Poland

Y. Chen
Suzhou Institute of Nano-Tech and Nano-Bionics (SINANO)
Chinese Academy of Sciences
385 Ruo Shui Road, Suzhou 215123, P. R. China

J. Gunasekera
Department of Mechanical and Mechatronic Engineering
Southern Illinois University
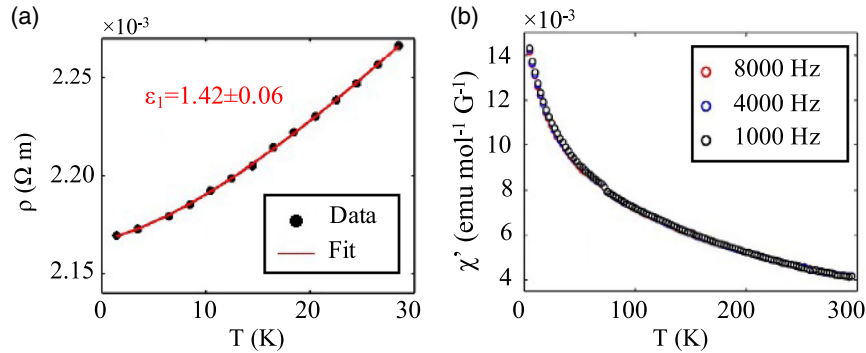Edwardsville, IL 62026, USA

Figure 1. a) Electrical resistivity as a function of temperature in $CaRuO_3$, depicting non-Fermi-liquid state at low temperature. The resistivity data is fitted using the power-law equation, $\rho = T^\varepsilon$, with fitted value of $\varepsilon = 1.42(0.06)$. b) Static susceptibilities at a few characteristic frequencies are plotted as a function of temperature. The static susceptibility exhibits paramagnetic behavior, which is ac frequency independent. (See also ref. [22].)

and crystalline specimens suggested a non-FL state in the system.[14] We performed detailed electrical and magnetic measurements on high-quality polycrystalline $CaRuO_3$ to further understand the unusual behavior.[22] Details about the sample synthesis can be found elsewhere.[22] We show electrical and magnetic measurements data in **Figure 1**. As we can see in Figure 1a, the experimental data are well described by a power-law expression, $\rho \propto T^\varepsilon$. The fitting parameter ε is found to exhibit a non-integer value of 1.42(0.06) below $T \approx 30$ K; illustrating a non-Fermi-liquid (NFL) state at low temperature. This is consistent with previous observations on the high-quality specimens of $CaRuO_3$. Electrical resistivity is also found to be independent of magnetic field application, suggesting a robust NFL state. The plot of the real part of magnetic susceptibility χ' in Figure 1b reveals the paramagnetic behavior with a small cusp around $T \approx 80$ K. A similar phenomenon was previously attributed to the onset of a long-range magnetic order.[16] However, no signature of any magnetic order was observed in elastic neutron scattering measurements.[22] Bulk static susceptibilities are also found to be independent of AC measurement frequency, hence ruling out the occurrence of the spin glass state in the system.

The ground state of $CaRuO_3$ is still a puzzle. No signature of antiferromagnetic or ferromagnetic order has ever been detected in this system in neutron scattering or magnetic measurements. Experimental investigation of dynamic behavior using inelastic neutron scattering measurements has revealed low energy excitation of short-range correlated spins at low temperature, see **Figure 2**. The dynamic correlation of Ru^{4+} ions does not exhibit any magnetic field dependence as no change in spectral weight is detected up to $H = 10$ T of magnetic field application (Figure 2b). It suggests a highly robust nature of magnetic fluctuation in $CaRuO_3$, which is also consistent with the previous NMR measurements.[27] Previously, we investigated the spin fluctuation rate and its temperature dependence using the quantitative analysis of inelastic neutron spectra.[22] In a first observation, a quasi-critical state, characterized by the divergence of relaxation time and the short-range critical scaling of dynamic susceptibility, was inferred to persist at low temperature. Perhaps. the prevalent quantum mechanical spin dynamics prohibits the development of a static order in this compound. Clearly, the ground state in $CaRuO_3$ is more exciting than previously understood. Recently, it
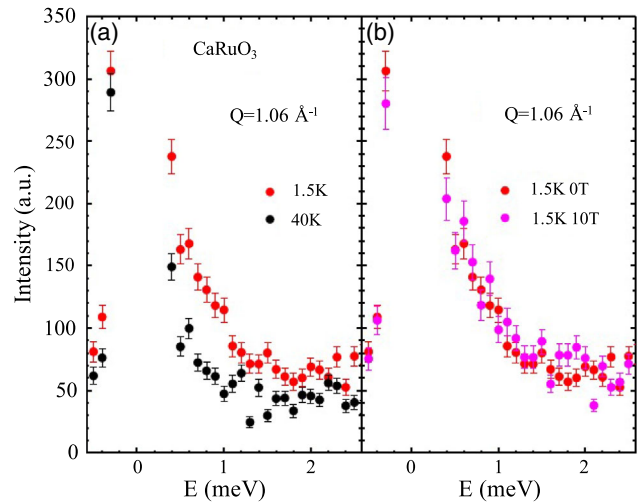

Figure 2. Plot of inelastic neutron scattering intensity as a function of energy transfer E ($E_i - E_f$) at: a) two different temperatures of $T = 1.5$ and 40 K in zero magnetic field, and b) at two different magnetic fields of $H = 0$ and 10 T at $T = 1.5$ K. Inelastic measurements were performed at fixed Q of 1.06 Å^{-1}. Additional spectral weight is detected below $E = 1$ meV in zero field measurement. Inelastic data remains unaffected to magnetic field application.

was revealed that the local criticality, including the NFL behavior, can be accessed by tuning the spin–orbital coupling (SOC) strength in perovskites.[28] The SOC tuning is argued to freeze the total momentum in systems with $J_{eff} = 1/2$, which serves as the boundary between FL and NFL behaviors.

2. Magnetic Fluctuation Mediated Metal-to-Insulator Transition in Chemically Substituted Ca(M_xRu$_{1−x}$)O$_3$, M = Ir, Co

MIT in magnetic materials has been a subject of intense study.[29] The transition is often accompanied by a change in the underlying magnetic characteristics, namely the transition from ferromagnetic to antiferromagnetic states or the onset of magnetic

fluctuations in the metallic state.[21,29] In strongly correlated electron systems, the MIT is argued to transition from the Hubbard model to the Heisenberg regime, where electrical conductivity is found to exhibit activated insulating behavior. Understanding the role of magnetic fluctuation in MIT is also enticing from the perspective of high-temperature superconductors, where the mechanism is argued to facilitate the Cooper pair formation.[30] We have investigated this problem in 113-ruthenate perovskite. For this purpose, Ru ions are substituted by Ir and Co ions in $CaRuO_3$ compound.

2.1. Study of $Ca(Ir_xRu_{1-x})O_3$

Since both $CaRuO_3$ and $CaIrO_3$ crystallize in the orthorhombic structure and manifest empty e_g-band electronic configurations of $4d^4$ (near half-filled) and $5d^5$ (half-filled) states in Ru^{4+} and Ir^{4+} ions, respectively, the experimental efforts provide direct insight into this problem.[23] Moreover, $CaIrO_3$ is known to manifest antiferromagnetic order below $T_N \approx 110$ K.[21,31] Thus, the end compounds represent two diverse magnetic systems. Substitution of Ru ion by Ir ion induces a metal-to-insulator transition. The electrical transport measurement data are shown in **Figure 3**a. Here, the normalized electrical resistivity (ρ/ρ_{300K}), where ρ_{300K} is the resistivity at $T = 300$ K) is plotted as a function of temperature for various chemical substitution coefficient x. As we can see, a gradual evolution from the metallic state, $x = 0$, to a strongly insulating state, $x = 1$, is detected as the coefficient x varies from 0 to 1. The paramagnetic characteristic of $CaRuO_3$ prevails across the low chemical substitution of Ru by Ir.

To understand the metal-to-insulator transition process, we have also performed detailed dynamic susceptibility measurements as a function of temperature and AC frequency for various substitution coefficients. The AC frequency varies from 10^2 Hz to 10^4 Hz, which corresponds to the magnetic fluctuation time scale of $t \geq 100\,\mu s$. Experimental results are presented in the form of contour plots of dynamic susceptibilities in Figure 3b. In this figure, we see that at $x = 1$, the plot is characterized by a singular

line at $T \simeq 110$ K, indicating the absence of dynamic behavior. At $x = 1$, the compound $CaIrO_3$ is a strong antiferromagnetic Mott insulator with no obvious dynamic properties at a long time scale. As × decreases below 0.7, the small regime of large χ'' at high frequency and low temperature extends to a higher temperature, thus illustrating significant spin dynamics in compounds with coefficient $x < 0.7$. In fact, the dynamic response to the AC susceptibility measurements is found to be strongest in $x = 0.3$ composition. Direct comparison of contour plots with electrical transport data (Figure 3a) reveals a one-to-one correspondence between the development of magnetic fluctuation and the onset of metallic behavior. At $x = 0$, the compound $CaRuO_3$ is a non-FL metal with strongly dynamic magnetic properties, characterized by fluctuating Ru spins. The synergistic experimental investigation of electrical and magnetic properties suggests the presence of magnetic fluctuations in various compositions of $Ca(Ir_xRu_{1-x})O_3$ perovskites.[23] The Ir-ion substitution of Ru-ion is found to enhance the Curie–Weiss temperature Θ_{CW} from -148 to -407 K and decreases Curie–Weiss constant C. Thus, the ordered moment decreases from $2.56\,\mu_B$ (in $CaRuO_3$) to $1.72\,\mu_B$ in $x = 1$ composition ($CaIrO_3$).[23]

2.2. MIT in $Ca(Co_xRu_{1-x})O_3$

While the study of $Ca(Ir_xRu_{1-x})O_3$ has provided valuable insights in understanding the novel MIT phenomena in 113-ruthenate perovskite, theoretical calculations hinted that substitution of Ru ion by isoelectronic Co-ion can lead to the formation of the artificial spin-1/2 state in $Ca(Co_xRu_{1-x})O_3$.[24] Moreover, the non-stoichiometric composition of calcium ruthenate also manifests a strong MIT process, see **Figure 4**. Detailed study of electrical and magnetic properties of $Ca(Co_xRu_{1-x})O_3$ showed that the MIT is comprised of both Hubbard and Heisenberg formalisms due to band filling.[29] At a low substitution coefficient of $x < 0.15$, the system still exhibits weak conducting characteristics—perhaps on the verge of becoming an insulator. Above $x = 0.15$, the electrical resistance is described by the
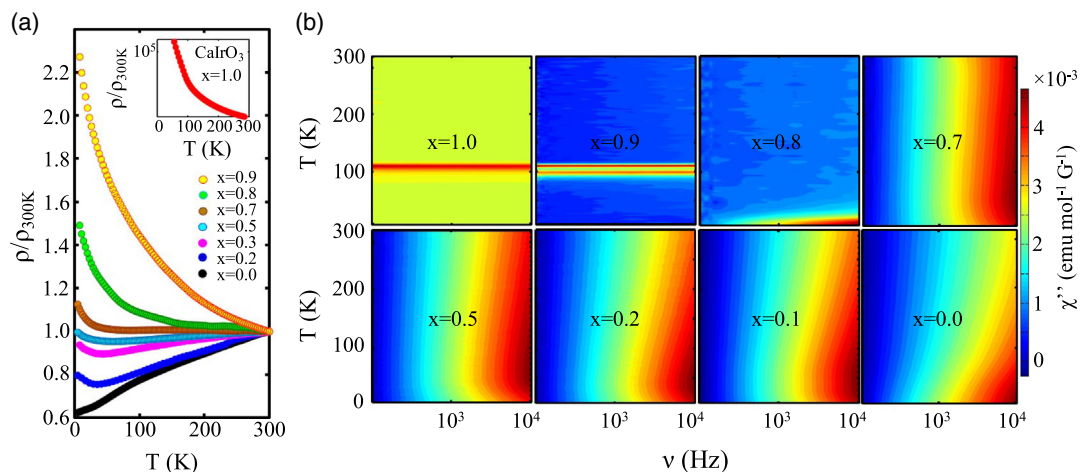

Figure 3. a) Metal-to-insulator transition as a function of x in $Ca(Ir_xRu_{1-x})O_3$. As x increases above 0.7, insulating behavior starts dominating. At $x = 1$, the compound $CaIrO_3$ is a strong Mott insulator. b) Temperature versus frequency plots of dynamic susceptibility, χ' for several chemical substitution coefficient x. For $x \leq 0.7$, strong frequency dependence of the dynamic susceptibilities are clearly observable, indicating significant magnetic fluctuations in the system. The onset of magnetic fluctuation coincides with the onset of metallic behavior in $Ca(Ir_xRu_{1-x})O_3$. (See also ref. [23].)
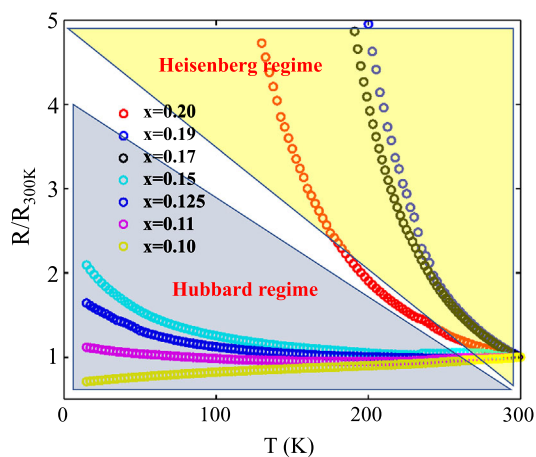
Figure 4. MIT in Co-doped $CaRuO_3$. Here, we show the plot of electrical resistivity versus temperature for various substitution coefficients x. As x increases, a transition from metal to insulator phase is clearly observed. At $x = 0.15$, the system is on the verge of becoming an insulator. Above $x = 0.15$, the plot of electrical resistivity suggests insulating characteristics.

Arrhenius formula, thus exhibiting activated behavior that is typically found in insulating materials. The localized Co-moments are described by Heisenberg formulation. Interestingly, the Co–Co interaction dominates the Ru–Co or Ru–Ru interaction in $Ca(Co_xRu_{1-x})O_3$.[24]

3. Localized Excitations in Ca(Co$_x$Ru$_{1-x}$)O$_3$

The substitution of Ru ion by Co ion generates a random distribution of artificial spin-1/2 moments. As described schematically in **Figure 5**, we have found that Co-substitution in $x = 0.17$ composition tends to create multiple exchange interaction pathways between neighboring and further away ions with ordered moment to the tune of $\approx 1 \mu_B$. Co impurities in the $CaRuO_3$ host are modeled within the coherent potential approximation. In this approach, a cluster with impurity atoms and the environment is incorporated into the host matrix in the real space representation.[24] Co impurity moment in $CaRuO_3$ host is estimated using the density functional theory calculations of the spin density of

opposite polarity. The artificial or quasi spin-1/2 of Co ion can develop liquid-like short-range dynamic correlation at low temperature. Elastic and inelastic neutron scattering measurements, performed on multi-axis crystal spectrometer (MACS) at the NIST Center for Neutron Research, revealed singlet-to-triplet transition between the entangled artificial spin-1/2 moments at low temperature of $T = 0.08$ K, see **Figure 6**. No magnetic order is detected in any of the stoichiometric compositions studied so far in $Ca(Co_xRu_{1-x})O_3$, $0 < x < 0.22$. Fitting of high-temperature magnetic susceptibility data has revealed an increasing trend in Θ_{CW}, from -148 to -219 K, and decreases Curie–Weiss constant C as the substitution coefficient increases. Consequently, the estimated ordered moment decreases from $2.56 \mu_B$ in $x = 0$ composition to $2.1 \mu_B$ in $x = 0.22$ composition.[24] Figure 6a shows the plot of background corrected and thermally balanced Q–E spectra at $T = 80$ mK and in zero magnetic field. We observe the well-defined localized excitations at $E = 5.9$ meV at $Q = 1$ Å^{-1} and $Q = 2$ Å^{-1}. The weak spectral weight at $Q = 2$ Å^{-1} can be accounted for due to the Co form factor. It is important to point out that no such localized excitation was observed in $CaRuO_3$ or $Ca(Co_xRu_{1-x})O_3$ with low substitution coefficient, which further corroborates the dominant role of Co^{4+}–Co^{4+} interaction in the gapped excitation. For quantitative analysis, we plot the averaged intensity of the inelastic spectra between $E = 4.5$ and 7.5 meV as a function of wave-vector Q at various temperatures in Figure 6b. The width of the peaks is much broader than the instrument resolution, indicating the short-range nature of dynamic correlations. The integrated intensity versus Q is well described by the singlet-to-triplet transition,[32] given by $I(Q) = |F(Q)|^2 \sum m_i^2 [1 - \sin(Qd_i)/(Qd_i)]$ where d_i, is the distance between neighboring ions and m_i is ordered moment, at $T = 80$ mK. The fitting involves not just the nearest neighbor spins, but also the next nearest neighbor spins. The estimated values of d_i, $d_1 = 3.85$ Å and $d_2 = 5.4$ Å are remarkably close to the actual lattice parameter values. It suggests that the collective excitation, indicating quantum fluctuation at low temperature, percolates beyond the nearest neighbors. Such behavior is typically observed in resonant valence bond candidate materials in spin liquid state.[33] However, in some cases, the disorder due to site switching impurity in RVB candidate materials has caused concern among the
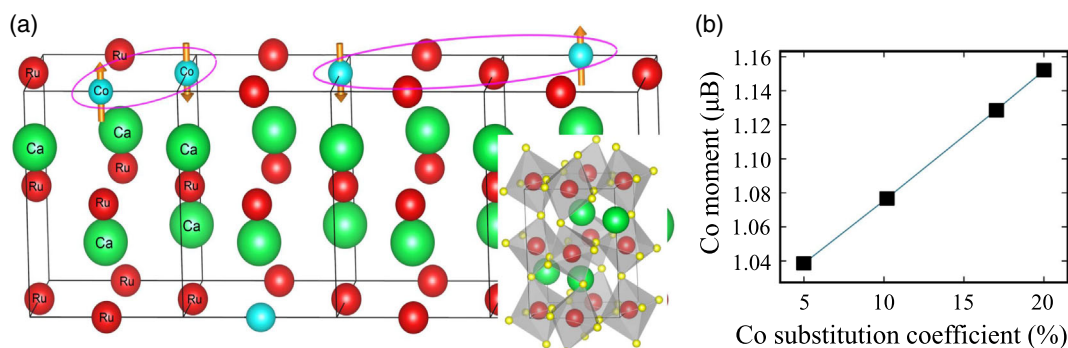

Figure 5. a) Schematic depiction of Ru substitution by Co ion at random sites. Co ion assumes spin-1/2 configuration and interacts with neighboring and further away ions. b) Theoretically calculated moment of Co^{4+} ion is found to be in the tune of $\approx 1 \mu_B$. Adapted under the terms of a Creative Commons Attribution International License.[24] Copyright 2018, The Authors, published by Wiley-VCH.
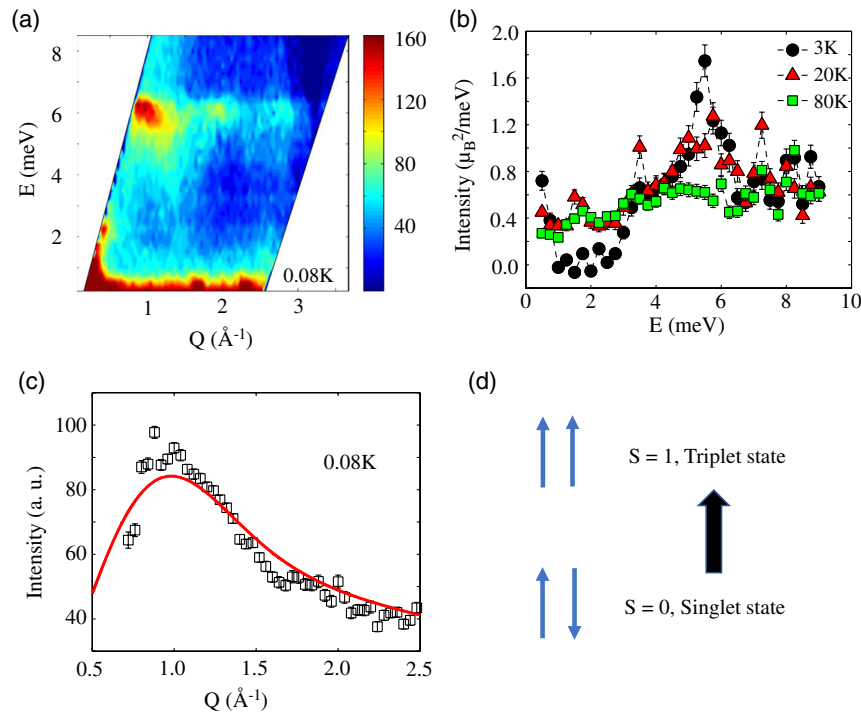
Figure 6. a) Energy–momentum (Q–E) map, depicting localized excitation in $Ca(Co_{0.17}Ru_{0.83})O_3$, at $T = 0.08$ K. b) Energy scan at fixed Q of 1.15 Å^{-1} at various temperatures. c) Plot of integrated intensity between $E = 4.5$ and 7.5 meV versus Q. Experimental data is well described by the singlet-to-triplet transition due to the dimer–dimer interaction between nearest and further away spins, as described in Figure 5a. d) Schematic description of singlet to triplet transition. We note that the triplet state is made of three states. However, for the illustration purpose, we are showing the transition between the singlet state and a triplet state. (a)–(c) Reproduced under the terms of a Creative Commons Attribution International License.[24] Copyright 2018, The Authors, published by Wiley-VCH.

scientific community.[34] According to one school of thought, the quantum fluctuation at low temperature is attributed to the disorderness in 2D frustrated lattice.

4. Dispersive Excitation at Higher Doping Percentage in $Ca(Co_xRu_{1-x})O_3$

To understand the evolution of spin dynamics in $Ca(Co_xRu_{1-x})O_3$ as a function of substitution coefficient x, we have further investigated the dynamic properties of Co^{4+} ions in the insulating regime. Detailed inelastic neutron scattering measurements were performed on $Ca(Co_{0.2}Ru_{0.8})O_{33}$ with $x = 0.2$. Unlike the observation of localized excitation in $x = 0.17$ compound, a dispersive magnetic excitation behavior is detected in $x = 0.2$ composition despite the absence of any magnetic order in the system. Plots of inelastic neutron data are shown in **Figure 7**. As we can see in the figure, the dispersive excitation at a low temperature of $T = 5$ K tends to ebb as temperature increases. At $T = 150$ K, the spin dynamics becomes much weaker with broad Q-dependence. It suggests that the correlated fluctuations, causing a dispersive excitation, break into weak short-range dynamic correlation as temperature increases.
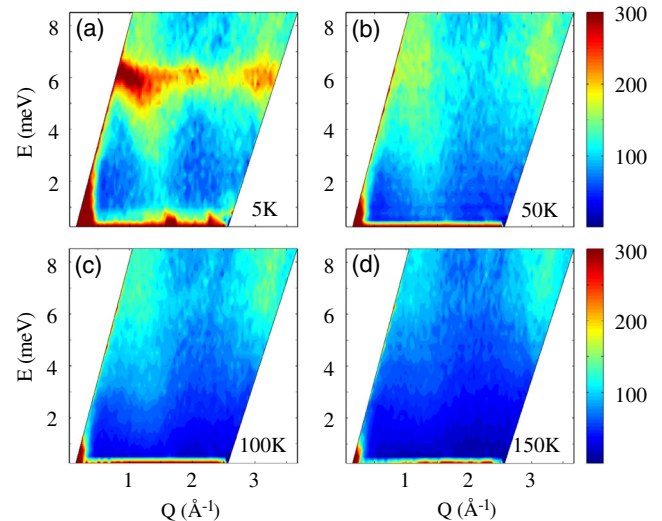

Figure 7. a) Q–E map obtained on MACS in $Ca(Co_{0.2}Ru_{0.8})O_3$ compound at $T = 5$ K. Localized excitation evolves into a dispersive behavior at a higher substitution coefficient of $x = 0.2$. b,c) The dispersive behavior weakens as temperature increases. d) At $T = 150$ K, weak remnants of spin dynamics with broad Q-dependences are detected.

5. Quantum Continuum Fluctuation Deep Inside the Spin Glass State in Optimally Doped $Ca(Co_{0.15}Ru_{0.85})O_3$

The MIT in cobalt-doped $CaRuO_3$ exhibits two distinct electrical transport regimes across the critical doping of $x = 0.15$. At $x = 0.15$, the system is found to manifest a weak spin glass state below $T_G \approx 23K$ with strong quantum continuum fluctuation at low temperature.[25] Given the fact that the spin freezing and quantum fluctuation are at the two opposite extremes in a correlated electron system, the experimental observation is highly peculiar in nature. Magnetic measurements using AC susceptibility analysis technique exhibits weak AC frequency-dependent cusp around $T_G = 23$ K, see **Figure 8**a,b. At $T > 23$ K, the static susceptibility depicts paramagnetic behavior, as a modest increase in χ' is detected between $T = 300$ and 2 K. However, below $T \approx 22$K, the weak AC frequency-dependent cusp in χ', coupled with the concurrent frequency-dependent enhancement in χ'', hints of the glassiness in the system. Similar phenomena are often observed in spin-glass-type systems.[35] However, the spin glass state is not prominent, which could be attributed to the competing spin fluctuations in the system. The presence of spin glass state in Co-doped $CaRuO_3$ compound is also confirmed by multiple reports, albeit at different doping percentages.

The study of spin dynamics in $Ca(Co_{0.15}Ru_{0.85})O_3$ is performed using inelastic neutron scattering measurements on high-quality polycrystalline material. Figure 8c,d shows the $Q - E$ maps at $T = 1.5$ K and $T = 300$ K. Experimental data are background corrected and thermally balanced. At $T = 1.5$ K, we notice that the entire energy–momentum space is occupied by the dynamic spectrum of the system. In fact, the system

manifests gapless continuous spin fluctuations to at least $E = 11.25$ meV, which is the maximum accessible energy on the MACS instrument at NIST. The gapless continuum excitation at low temperature is quantum mechanical in nature, as the broad spin fluctuation tends to subside as temperature increases, see Figure 8e. At $T = 300$ K, the dynamic behavior tends to disappear. It suggests that the spin dynamics of Co^{4+} ions are local in nature that are reflected in the quantum continuum fluctuation. This argument is verified using the scaling analysis of dynamic susceptibility where the small scaling coefficient of $\alpha \approx 0.1$ was inferred to reveal the extreme locality resulting in near Q-independence scaling.[25] Most surprisingly, the continuum fluctuation coexists with the spin glass state in $Ca(Co_{0.15}Ru_{0.85})O_3$. Unlike a conventional spin glass system where the spin freezing is well pronounced below the glass transition temperature, $Ca(Co_{0.15}Ru_{0.85})O_3$ manifests a weak glassy character. We argue that the strong spin fluctuations at a low temperature significantly weakens the relaxation time of the nascent glassy phase and prohibits it from developing a static order. As we mentioned previously, no trace of any type of magnetic order is detected in the system.

In summary, we have presented an overview of electrical and magnetic properties in stoichiometric and chemically doped $CaRuO_3$ perovskite. Ruthenate perovskite provides a rich platform to study many facets of quantum magnetism that are at the frontier of condensed matter physics research. In the stoichiometric composition, the parent compound exhibits a non-FL behavior with a complex magnetic ground state. The system is on the verge of ferromagnetic ordering. Yet, the dynamic nature of spin correlation prohibits the development of long-range magnetic order. Chemical substitution on the Ru site by Ir and Co ions reveals metal-to-insulator transition as a function of the substitution coefficient. While the MIT process due to
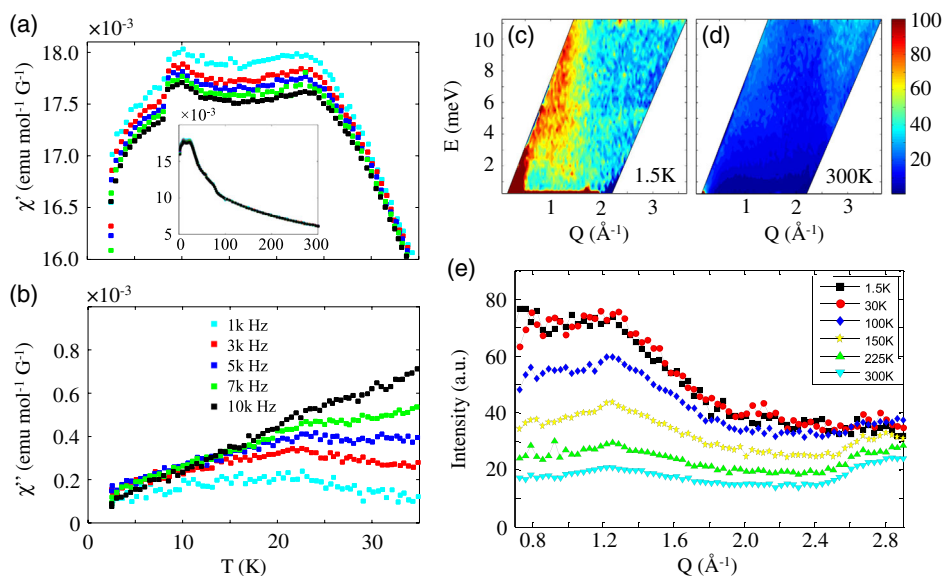

Figure 8. a,b) AC frequency dependent plots of static and dynamic susceptibilities in critically doped $Ca(Co_{0.15}Ru_{0.85})O_3$ compound. A weak spin glass behavior is detected in this system. c,d) Interestingly, a coexistence of glassy behavior with continuum fluctuation is detected in $Ca(Co_{0.15}Ru_{0.85})O_3$ at low temperature. As temperature increases, the quantum continuum fluctuation subsides. e) Plot of averaged intensity from $E = 2.5$ to 9.5 meV versus Q. Broad excitation in Q is detected at low temperature. As temperature increases, neutron spectral weight becomes indistinguishable from the background. (a)–(d) Reproduced with permission.[25] Copyright 2019, Elsevier.

Ir substitution is found to be mediated by the underlying magnetic fluctuation, the Co substitution causes a host of new phenomena that resemble to the resonant valence bond physics. Most surprisingly, a coexistence of the weak spin glass phase with the quantum continuum state is detected in the critically doped $Ca(Co_{0.15}Ru_{0.85})O_3$ compound. It can be argued that the disorder due to Co substitution be causing the glassy behavior and extreme locality, responsible for the continuum fluctuation, in the system. However, the same disorder, albeit at a nominally higher level, induces localized excitation, followed by the magnetic dispersive behavior at low temperature. Thus, the puzzling behavior of quantum continuum fluctuation in the spin glass state, which occurs in a material at the crossroad of Hubbard and Heisenberg formalism, poses new challenge to our understanding of the quantum magnetism. A related question is, does the disorder play important role in quantum fluctuation. Perhaps, future research works on the single crystal specimen can shed light on this pertinent problem.

Conflict of Interest

The authors declare no conflict of interest.

Data Availability Statement

The data that support the findings of this study are available from the corresponding author upon reasonable request.

[1] C. M. Varma, S. Schmitt-Rink, E. Abrahams, *Solid State Commun.* **1987**, *62*, 681.
[2] J. G. Bednorz, K. A. Muller, *Z. Phys. B: Condens. Matter* **1986**, *64*, 189.
[3] A. P. Ramirez, *J. Phys.: Condens. Matter* **1997**, *9*, 8171.
[4] Y. Yu, P. Karayaylali, S. Nowak, L. Giordano, M. Gauthier, W. Hong, R. Kou, Q. Li, J. Vinson, T. Kroll, D. Sokaras, C. Sun, N. Charles, F. Maglia, R. Jung, Y. Horn, *Chem. Mater.* **2019**, *19*, 7864.
[5] U. Schollwok, J. Richter, D. Farnell, R. Bishop, *Quantum Magnetism (Lecture Notes In Physics)*, Springer, Berlin Heidelberg **2004**.
[6] L. Balents, *Nature* **2010**, *464*, 199.
[7] R. Coldea, D. Tennant, A. M. Tsvelik, Z. Tylczynski, *Phys. Rev. Lett.* **2001**, *86*, 1335.
[8] X. Deng, K. Haule, G. Kotliar, *Phys. Rev. Lett.* **2016**, *116*, 256401.
[9] N. Kikugawa, L. Balicas A. P. Mackenzie, *J. Phys. Soc. Jpn.* **2009**, *78*, 014701.
[10] J. M. Longo, P. M. Raccah J. B. Goodenough, *J. Appl. Phys.* **1968**, *39*, 1327.
[11] G. Cao, S. McCall, M. Shepard, J. E. Crow, R. P. Guertin, *Phys. Rev. B* **1997**, *56*, 321.
[12] T. He, R. J. Cava, *J. Phys.: Condens. Matter* **2001**, *13*, 8347.
[13] I. I. Mazin, D. J. Singh, *Phys. Rev. B* **1997**, *56*, 2556.
[14] G. Cao, O. Korneta, S. Chikara, L. E. DeLong, P. Schlottmann, *Solid State Commun.* **2008**, *148*, 305.
[15] P. Khalifah, I. Ohkubo, H. M. Christen, D. G. Mandrus, *Phys. Rev. B* **2004**, *70*, 134426.
[16] I. Felner, I. Nowik, I. Bradaric, M. Gospodinov, *Phys. Rev. B* **2000**, *62*, 11332.
[17] H. Mukuda, K. Ishida, Y. Kitaoka, K. Asayama, R. Kanno, M. Takano, *Phys. Rev. B* **1999**, *60*, 12279.
[18] P. Kostic, Y. Okada, N. C. Collins, Z. Schlesinger, J. W. Reiner, L. Klein, A. Kapitulnik, T. H. Geballe, M. R. Beasley, *Phys. Rev. Lett.* **1998**, *81*, 2498.
[19] Y. S. Lee, J. Yu, J. S. Lee, T. W. Noh, T.-H. Gimm, H.-Y. Choi, C. B. Eom, *Phys. Rev. B* **2002**, *66*, 041104.
[20] L. Klein, L. Antognazza, T. H. Geballe, M. R. Beasley, A. Kapitulnik, *Phys. Rev. B* **1999**, *60*, 1448.
[21] J. Gunasekara, Y. Chen, J. Kremenak, P. F. Miceli, D. K. Singh, *J. Phys.: Condens. Matter* **2015**, *27*, 052201.
[22] J. Gunasekera, L. Harriger, T. Heitmann, A. Dahal, H. Knoll, D. K. Singh, *Phys. Rev. B* **2015**, *91*, 241103.
[23] J. Gunasekera, L. Harriger, A. Dahal, T. Heitmann, G. Vignale, D. K. Singh, *Sci. Rep.* **2015**, *5*, 18047.
[24] J. Gunasekera, A. Dahal, Y. Chen, J. A. Rodriguez-Rivera, L. W. Harriger, S. Thomas, T. W. Heitmann, V. Dugaev, A. Ernst, D. K. Singh, *Adv. Sci.* **2018**, *5*, 1700978.
[25] Y. Chen, A. Dahal, J. A. Rodriguez-Rivera, G. Xu, T. W. Heitmann, V. Dugaev, A. Ernst, D. K. Singh, *Mater. Today Phys.* **2020**, *12*, 100163.
[26] H. Kojitani, Y. Shirako, M. Akaogi, *Phys. Earth Planet. Interiors* **2007**, *165*, 127.
[27] K. Yoshimura, T. Imai, T. Kiyama, K. R. Thurber, A. W. Hunt, K. Kosuge, *Phys. Rev. Lett.* **1999**, *83*, 4397.
[28] A. Kim, H. Jeschke, P. Werner, R. Valentí, *Phys. Rev. Lett.* **2017**, *118*, 086401.
[29] M. Imada, A. Fujimori, Y. Tokura, *Rev. Mod. Phys.* **1998**, *70*, 1039.
[30] P. Lee, N. Nagaosa, X. Wen, *Rev. Mod. Phys.* **2006**, *78*, 17.
[31] M. Moretti Sala, K. Ohgushi, A. Al-Zein Y. Hirata, G. Monaco, M. Krisch, *Phys. Rev. Lett.* **2014**, *112*, 176402.
[32] M. Mourigal, W. T. Fuhrman, J. P. Sheckelton, A. Wartelle, J. A. Rodriguez-Rivera, D. L. Abernathy, T. M. McQueen, C. L. Broholm, *Phys. Rev. Lett.* **2014**, *112*, 027202.
[33] M. Lawler, A. Paramekanti, Y. Kim, L. Balents, *Phys. Rev. Lett.* **2008**, *101*, 197202.
[34] T. Han, J. Helton, S. Chu, D. Nocera, J. Rodriguez, C. Broholm, Y. S. Lee, *Nature* **2012**, *492*, 406.
[35] K. Binder, A. Young, *Rev. Mod. Phys.* **1986**, *58*, 801.